

Accurate calibration for a camera–projector measurement system based on structured light projection

Xiaobo Chen^a, Juntong Xi^{a,b,*}, Ye Jin^a, Jin Sun^a

^a*School of Mechanical Engineering, Shanghai Jiao Tong University, 1212 Haoran Building, 1954 Huashan Road, Shanghai 200030, China*

^b*State Key Laboratory of Mechanical System and Vibration, Shanghai Jiao Tong University, China*

Available online 18 January 2008

Abstract

The accurate calibration for a camera–projector measurement system based on structured light projection is important to the system measurement accuracy. This study proposes an improved systematic calibration method focusing on three key factors: calibration model, calibration artifact and calibration procedures. The calibration model better describes the camera and projector imaging process by considering higher to fourth order radial and tangential lens distortion. The calibration artifact provides a sufficient number of accurate 3D reference points uniformly distributed in a common world coordinate system. And the calibration procedures calibrate the camera and projector simultaneously based on the same reference points to eliminate the influences of the camera calibration error on the projector calibration. The experiments demonstrate that our calibration method can improve the measurement accuracy by 47%.
© 2007 Elsevier Ltd. All rights reserved.

Keywords: System calibration; Camera–projector measurement system; Structured light; Three-dimensional shape measurement

1. Introduction

The optical techniques for 3D shape measurement have been extensively studied and played an increasingly important role for various applications, such as quality control, archeology, virtual reality, industrial inspection, reverse engineering, etc. [1,2]. Some common techniques include stereo-vision [3,4], laser scanning [5,6], structured light [7,8], phase shifting [9], interferometry [10], Moiré [11] and so on. Among all these techniques, the triangulation with structured light projection is promising due to its advantages of fast speed, high accuracy, high spatial resolution, low cost, full field and easy implementation [12–14]. As shown in Fig. 1, a typical structured light measurement system consists of a camera and a projector. The projector projects a series of encoded vertical stripe patterns onto the object surface and the camera, which is at an angle to the illumination direction, records the distorted patterns caused by the depth variation of the surface. Hence, for the surface point, each camera pixel “sees”, it

has a corresponding stripe number determined by the image decoding at that pixel. Thus, the 3D surface point can be reconstructed based on triangulation providing that the system parameters have been obtained through the system calibration.

The key to an accurate 3D reconstruction for the structured light measurement system is the accurate calibration of the specific configurations of that system. This calibration is to estimate the unknown system parameters based on the system mathematical model according to some known calibration references. In order to ensure the system calibration accuracy, various factors need to be considered and controlled carefully during the calibration. And our work proposes an accurate and systematic calibration method with the improvements on three key factors: calibration model, calibration artifact and calibration procedures, as detailed separately below.

1.1. Calibration model

The calibration model, which includes the camera and projector models, describes the perspective projection from the 3D world to the 2D camera and projector image planes. And the calibration accuracy largely depends on how well

*Corresponding author. Tel.: +86 21 34206771; fax: +86 21 62932070.

E-mail addresses: xiaoboc@sjtu.edu.cn (X. Chen), jtxi@sjtu.edu.cn (J. Xi), yejin@sjtu.edu.cn (Y. Jin), sunjin1001@sjtu.edu.cn (J. Sun).

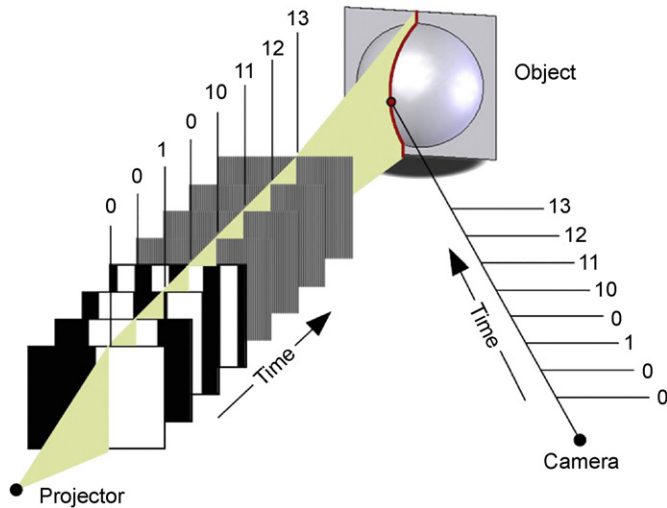


Fig. 1. A typical structured light system.

this calibration model can present the projection processes. In the past decades, the camera has been extensively studied and its modeling and calibration techniques have become very mature [15–18]. Normally, a nonlinear camera model considering both radial and tangential lens distortion high to fourth order is sufficient for a structured light measurement system [16]. The projector is claimed to be conceptually equal to camera acting in reverse, but it always adopts a reduced projection model instead. The reduced projector model normally rejects the lens distortion or just considers second order radial lens distortion. Even in some cases, a 1D projector model is also reasonable. The reason is because the projector projects the structured light encoded only in 1D, and the inverse projector model, which is essential for the 3D reconstruction, cannot be built from the 1D pixel position if there is no model reduction. However, these model reductions may degrade the system calibration accuracy thus limit the system measurement accuracy. In our previous work [19], we proposed a new 3D reconstruction method without the inverse projector model. This makes it possible to use a more accurate projector model the same as that of camera by considering high to fourth order radial and tangential lens distortion.

1.2. Calibration artifact

The calibration artifact provides sufficient number of 3D references for the system calibration. Some common calibration artifacts can be 1D lines [20], 2D planes [21] and 3D objects [17,22] with some known accurate reference points. During calibration, the artifact is placed in various poses to provide enough 3D reference points within the measurement volume. However, it is unavoidable that these reference points are normally distributed unevenly leading to the fact that the calibration error becomes larger in the space where there are less reference points. Moreover, each pose is associated with a new additional world coordinate system (WCS) to express the reference points at

that pose. This makes the calibrated transformations from camera to projector slightly different when they are obtained in different WCS because the calibration is accomplished in a sense of maximum likelihood. To make a compromise of all these different transformations to get a unique one, which is required for 3D reconstruction, can lead to some calibration error. In order to eliminate these two influences, we use a 2D flat board with evenly distributed circular marks translated along its normal with the aid of the accurate moving mechanism of a Replica/Reversa 3D laser scanner. Thus, the mark centers can construct an accurate 3D lattice of reference points, which are uniformly distributed within the measurement volume in one common WCS.

1.3. Calibration procedures

In most conventional calibration methods, the system calibration is separated into two sequenced procedures: camera calibration and projector calibration. The camera calibration is accomplished based on the reference data composed of the 3D reference points and their 2D camera correspondences extracted from the images. Unlike the camera calibration, the projector calibration normally prepares the reference data by projecting an extra calibration pattern with known 2D references to the calibration artifact in different poses and obtaining the 3D correspondences with the aid of the calibrated camera [14,23–25]. In this way, the camera calibration error unavoidably affects the reliability of the projector reference data thus degrades the accuracy of the projector calibration. And it is claimed that the resulted projector calibration error can reach 1-order magnitude larger than that of the camera [14]. Our calibration procedures are able to extract the 2D pixel correspondences of the same 3D reference points both on camera and projector image planes, thus making it possible to calibrate the camera and projector simultaneously to eliminate the influences of the camera calibration error on the projector calibration.

The rest of this paper is organized as follows. Section 2 presents the mathematical models used in our structured light measurement system. Section 3 describes the system calibration method. Particularly, Sections 3.1 and 3.2 describe calibration artifact and calibration procedures, respectively. Section 4 presents the experiments to evaluate the performance improvements of our calibration method. And Section 5 concludes this paper.

2. Mathematical models

2.1. Camera and projector model

The camera and projector are based on the same perspective projection model with high to fourth order radial and tangential lens distortion. As shown in Fig. 2, $\mathbf{P}_w = [X \ Y \ Z]^T$ is a point in WCS ($O-XYZ$), and it has the coordinates in the device coordinate system ($o-xyz$)

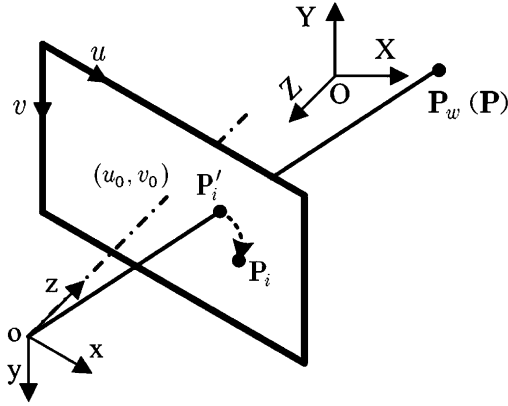


Fig. 2. Camera and projector model.

expressed by $\mathbf{P} = [x \ y \ z]^T$. It is a rigid body transformation from \mathbf{P}_w to \mathbf{P} , which can be expressed by

$$\mathbf{P} = \mathbf{R} \cdot \mathbf{P}_w + \mathbf{T}, \quad (1)$$

where \mathbf{R} and \mathbf{T} are the rotation and translation matrices, respectively.

Let \mathbf{P}_n be the projection of \mathbf{P} onto the normalized image plane, which is parallel to the image plane and is unit distance to the lens center O . Then, \mathbf{P}_n can be given by

$$\mathbf{P}_n = \begin{bmatrix} x_n \\ y_n \end{bmatrix} = \begin{bmatrix} \frac{x}{z} \\ \frac{y}{z} \end{bmatrix}. \quad (2)$$

Considering the influences of the radial and tangential lens distortion on \mathbf{P}_n , we have the distorted projection \mathbf{P}_d on the normalized image plane expressed by [16]

$$\mathbf{P}_d = f_d(\mathbf{P}_n, \mathbf{K}) = \begin{bmatrix} x_d \\ y_d \end{bmatrix} = \mathbf{P}_n + (k_1 r^2 + k_2 r^4) \mathbf{P}_n + \begin{bmatrix} 2k_3 x_n y_n + k_4(r^2 + 2x_n^2) \\ k_3(r^2 + 2y_n^2) + 2k_4 x_n y_n \end{bmatrix}, \quad (3)$$

where $r^2 = x_n^2 + y_n^2$ and $\mathbf{K} = [k_1 \ k_2 \ k_3 \ k_4]$ is the lens distortion coefficient. The last two terms in the right side of Eq. (3) stand for the radial and tangential lens distortion, respectively.

Then the projection on the image plane \mathbf{P}_i can be expressed as follows:

$$\mathbf{P}_i = \begin{bmatrix} u \\ v \end{bmatrix} = \begin{bmatrix} f_u x_d + u_0 \\ f_v y_d + v_0 \end{bmatrix}, \quad (4)$$

where f_u and f_v are the horizontal and vertical focal lengths, respectively, and u_0 and v_0 are the coordinates of the principle point.

In summary, the camera and projector model can be expressed as follows:

$$\mathbf{P}_i = g(\mathbf{P}_w, \Theta), \quad (5)$$

where $g(\cdot)$ describes the imaging process from WCS to the image plane and $\Theta = [\mathbf{R} \ \mathbf{T} \ f_u \ f_v \ u_0 \ v_0 \ \mathbf{K}]$ is the model parameter.

2.2. Light encoding

The projected light in the structured light measurement system is tracked by the combined encoding method of gray-code and four-step phase-shift [12–14]. As illustrated in Fig. 3(a), the n -bit gray-code encodes 2^n sets of light directions by projecting n successive stripe patterns. Although the gray-code has wide non-ambiguity spatial range, its resolution is rather low because of the limit of n . On the contrary, the four-step phase-shift achieves high spatial resolution but has the ambiguity problem [10]. When these two methods are combined, their negative features can be complemented to be able to measure even discontinuous surfaces with fine details. The details are explained below.

The four-step phase-shift encodes the projected light directions with phases by projecting four sinusoidal vertical stripe patterns with the intensities expressed by

$$I_q = I' + I'' \cos\left(\phi' + q \frac{\pi}{2}\right) \quad (q = 0, 1, 2, 3), \quad (6)$$

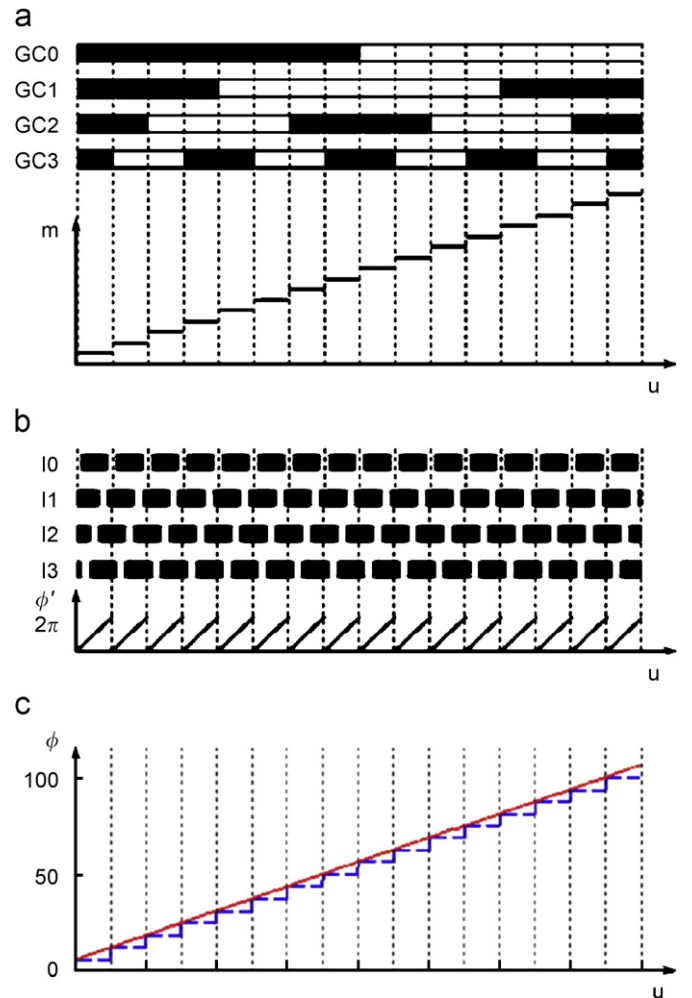


Fig. 3. Light encoding methods: (a) 4-bit gray-code, (b) four-step phase-shift, and (c) absolute phase by combining 4-bit gray-code and four-step phase-shift.

where I' is the average intensity, I'' is the intensity modulation and the principle phase ϕ' can be solved by algebraically combining Eq. (6):

$$\phi' = \arctan \frac{I_1 - I_3}{I_0 - I_2} + c, \quad (7)$$

where c is a correcting term extending the arc tangent value from $-\pi/2 \sim \pi/2$ to $0 \sim 2\pi$. As shown in Fig. 3(b), the principle phase ϕ' is linearly distributed within its period.

When the phase-shift period coincides with the gray-code edges, these two encoding methods can be combined and the obtained absolute phase ϕ is given by

$$\phi = 2\pi m + \phi', \quad (8)$$

where m is the stripe number defined by gray code. As shown in Fig. 3(c), the phase-shift works as the subdivision of gray-code and the absolute phase is distributed linearly and spatial continuously over the whole light projection directions. Thus, all the light directions are trackable by their absolute phases.

2.3. 3D reconstruction

The 3D reconstruction can be accomplished given the camera pixels and their absolute phases which are from the intensity decoding of the captured images. As shown in Fig. 4, the 3D point P_w is viewed by the camera pixel P_i^c and is illuminated by the projector pixel column $u_p = u_p^*$, which is determined from the absolute phase of P_i^c . If the lens distortion is ignored, P_w becomes simply the intersection of the ray defined by P_i^c and the plane defined by u_p^* . When the lens distortion is considered, the undistorted pixel of P_i^c , denoted by $P_i'^c$, needs to be obtained first. Since the high-order radial and tangential lens distortion is considered, there is no simple analytical solution to calculate $P_i'^c$ from P_i^c . An inverse camera model is proposed in Refs. [16,26] to iteratively approximate $P_i'^c$. However, this inverse camera model is inapplicable to the projector since only 1D pixel position on the projector image plane is available. An alternative way is to reconsider the 3D reconstruction as to find the point lying on $O_c P_i^c$ which can also be projected to the projector pixel column u_p^* [19]. It becomes a nonlinear equation which can be solved

numerically by Newton–Raphson method [27] providing a good initial point. A sufficient good initial point is the intersection of $O_c P_i^c$ and the plane defined by u_p^* without considering the projector lens distortion. The detailed mathematical descriptions are attached in Appendix.

3. System calibration

The system calibration starts with the measurement of the calibration artifact, which provides a uniformly distributed 3D lattice of reference points throughout the measurement volume. And then it extracts the pixel correspondences of the reference points on the camera and projector image planes. These reference data can be fed into the system calibration model to estimate the system parameters using maximum likelihood estimation.

3.1. Calibration artifact

The calibration artifact in our research is illustrated in Fig. 5(a). A flat aluminum board is mounted on the high precision moving mechanism of a Replica/Reversa 3D laser scanner with its normal coinciding with the moving direction. This board is pasted with a calibration pattern with evenly distributed white circular mark array in black background. The board origin is defined to be located at the center of the central mark. And this origin can be recognized in the captured images by four identifiers, which are extra smaller circular marks composing a rectangle on the pattern. Since the relative positions of all the mark centers with respect to the origin are known, this board can provide a set of coplanar reference points. When the moving mechanism translates the board at the distance of the mark spacing for each step, a uniformly distributed 3D lattice of reference points which are in a common WCS and cover the whole measurement volume is obtained, as shown in Fig. 5(b). The WCS is defined as follows: its origin is located at the board origin when the board is translated to the middle of its moving range, O – XY plane is on the board with X , Y axes along the directions of the circular mark array, and Z axis is pointing opposite to the normal of the pattern. In this way, all the reference

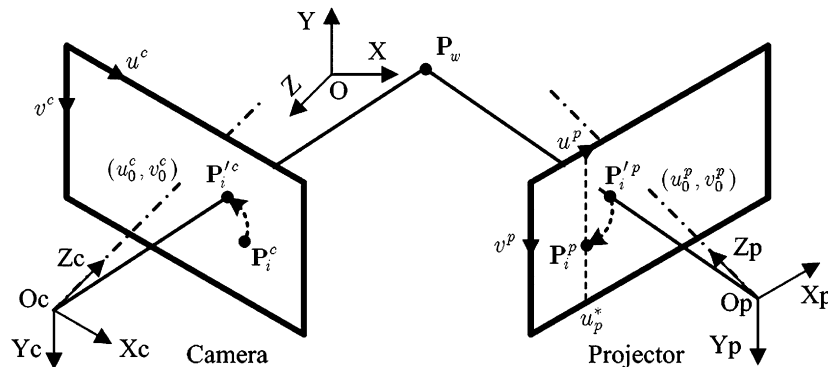


Fig. 4. System geometry for 3D reconstruction.

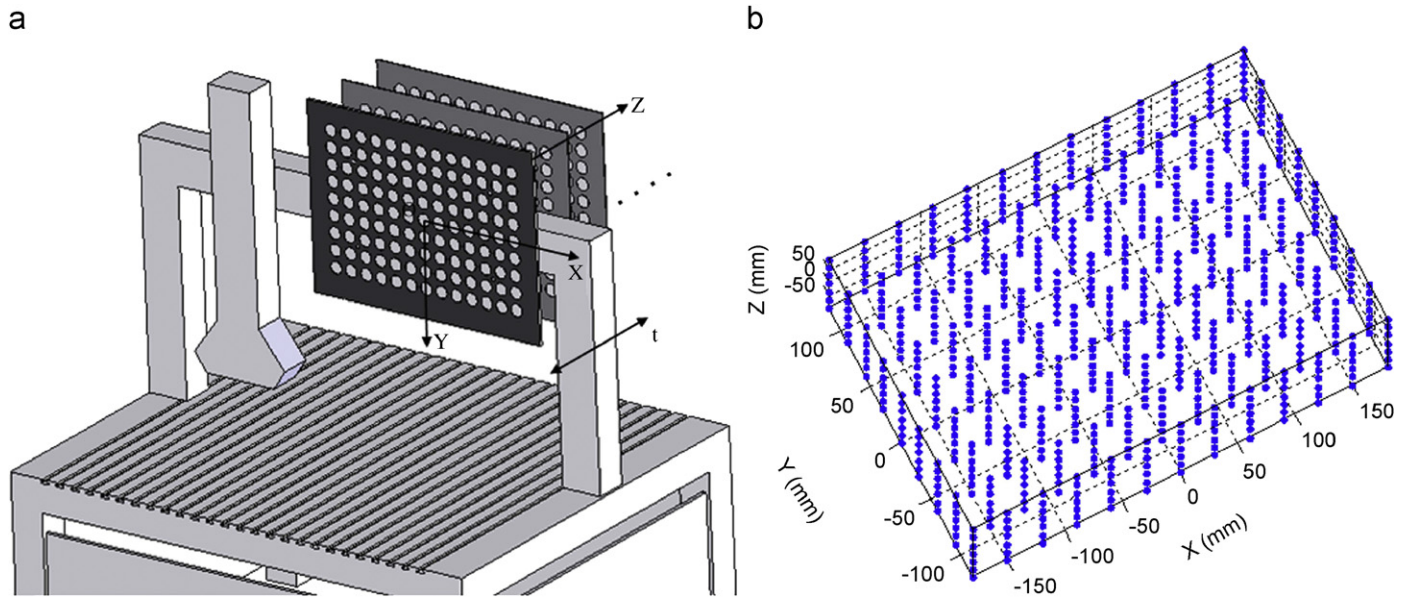


Fig. 5. Calibration artifact: (a) flat board translated along its normal direction and (b) uniformly distributed 3D lattice of reference points throughout the measurement volume.

points have their 3D coordinates expressed in one common WCS.

3.2. Calibration procedures

The calibration procedures to collect the reference data and estimate the system parameters are illustrated in Fig. 6. The reference data in our method includes the 3D coordinates of the reference points and their 2D pixel correspondences on the camera and projector image planes. For each translation of the calibration board, an image is captured with full illumination on that board and then is converted to binary. The circular mark regions on the image are detected and segmented by the connected region detection algorithm [28] and their centroids are calculated as the correspondences of the reference points. Besides, the region of the centroids of the four identifiers is also obtained to identify the board origin as well as determine the relative positions of all the centroids with respect to the origin. Thus, for each reference point in WCS denoted by $\mathbf{P}_w(k)$, where k is the index, its correspondence on the camera image plane $\mathbf{P}_c(k)$ can be determined according to its relative position to the origin.

The correspondences of the reference points $\mathbf{P}_w(k)$ on the projector image plane are obtained by means of encoding the projected light with the combination of gray-code and phase-shift in both horizontal and vertical directions. The projector projects sets of horizontal and vertical structured light patterns onto the board and the camera captures the scene images, from which the horizontal and vertical absolute phase maps can be constructed for all the camera pixels by Eqs. (7) and (8). So for each correspondence on the camera image plane $\mathbf{P}_c(k)$, it is assigned the horizontal and vertical absolute phases obtained by the bilinear

interpolation of the absolute phases of its four adjacent pixels. These horizontal and vertical absolute phases can be used to retrieve the sub-pixel row and column in the projector image plane which illuminates $\mathbf{P}_w(k)$ according to the encoding method. Thus, the correspondence on the projector image plane, denoted by $\mathbf{P}_p(k)$, can be uniquely determined by the intersection of the pair of sub-pixel row and column. Fig. 7 illustrates an example of the extracted correspondences for a single translation. Since no human interactions are required to locate the mark regions, which could be very tedious, the image processing and the correspondence extraction can be totally automatic. Once all the reference data is prepared, the system parameters can be further estimated by feeding these data into the calibration model, which is explained in Section 3.3.

3.3. System parameter estimation

The maximum likelihood estimation is adopted to obtain the system parameters with the reference data based on the calibration model. The objective function is to minimize the sum of the re-projection error of all the reference points onto the camera and projector image planes. This can be expressed by

$$\{\Theta_c, \Theta_p\} = \arg \min \sum_k (||g(\mathbf{P}_w(k), \Theta_c) - \mathbf{P}_c(k)||^2 + ||g(\mathbf{P}_w(k), \Theta_p) - \mathbf{P}_p(k)||^2), \quad (9)$$

where $\Theta_c = [\mathbf{R}_c \ \mathbf{T}_c \ f_u^c \ f_v^c \ u_0^c \ v_0^c \ \mathbf{K}_c]$, $\Theta_p = [\mathbf{R}_p \ \mathbf{T}_p \ f_u^p \ f_v^p \ u_0^p \ v_0^p \ \mathbf{K}_p]$ are the camera and projector parameters, respectively. It is a nonlinear optimization problem which can be solved iteratively by the Levenberg–Marquardt method [27] providing a good initial guess. This

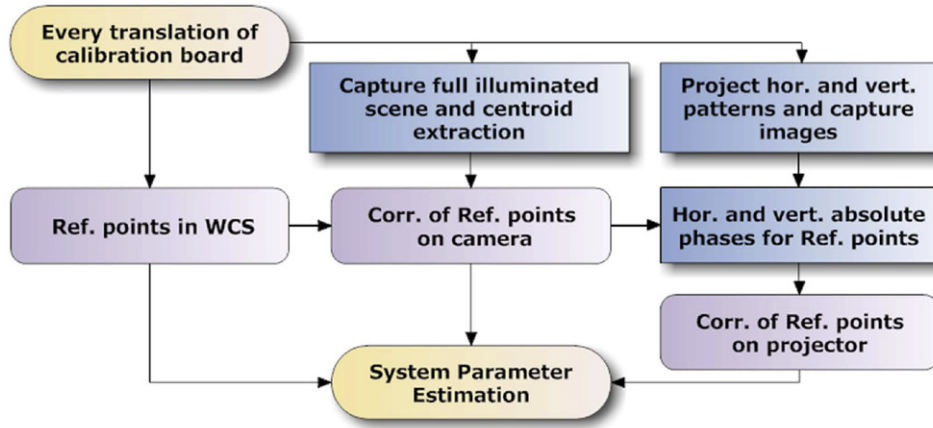


Fig. 6. Flowchart of the system calibration procedures.

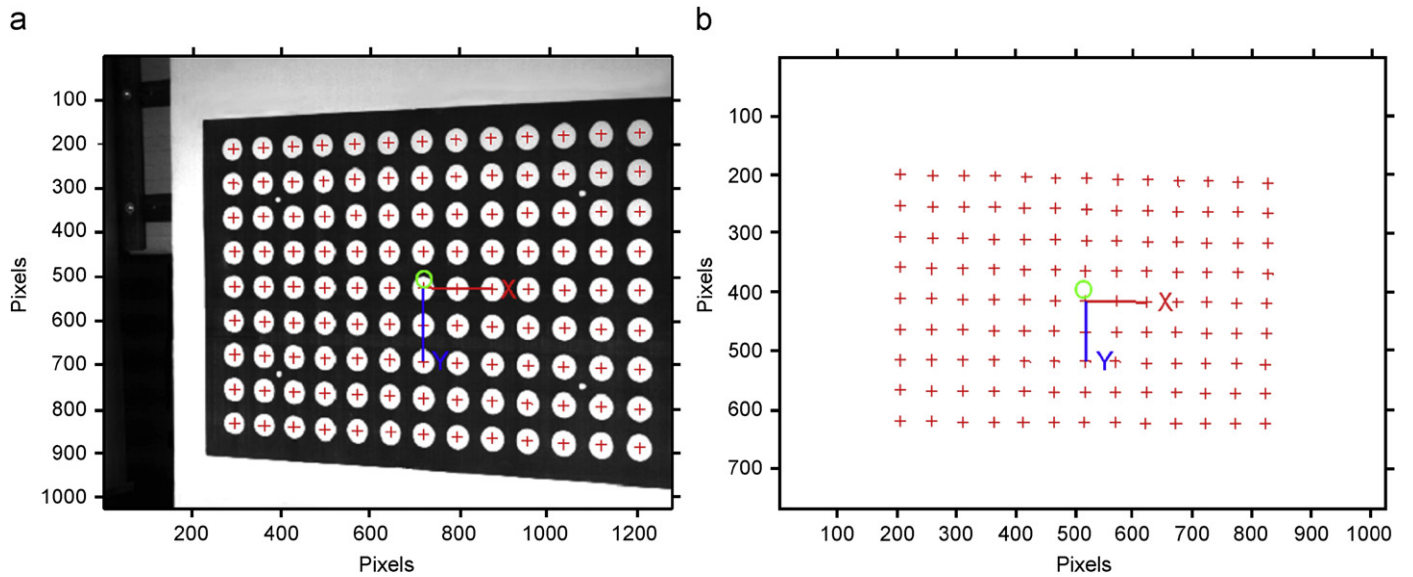


Fig. 7. Extracted correspondences of the reference points on the device image planes: (a) camera and (b) projector.

initial guess can be given by estimating the parameters of the camera and projector individually based on a linear device model discarding the lens distortion. Thus, the close form solution of the initial guess can be obtained by the linear least-squares fitting method.

Once the rotation and translation matrices of the camera and projector \mathbf{R}_c , \mathbf{T}_c and \mathbf{R}_p , \mathbf{T}_p are obtained, the rotation and translation from the camera to the projector, denoted by \mathbf{R}_{pc} and \mathbf{T}_{pc} can be given as follows:

$$\mathbf{R}_{pc} = \mathbf{R}_p(\mathbf{R}_c)^{-1}, \quad (10)$$

$$\mathbf{T}_{pc} = \mathbf{T}_p - \mathbf{R}_p(\mathbf{R}_c)^{-1}\mathbf{T}_c \quad (11)$$

3.4. Error correction for centroid extraction

It should be aware that previously we extracted the centroids of the mark regions as the correspondences of the reference points on the camera image plane. However,

these two are generally deviated due to the perspective distortion [7,22]. And this deviation leads to the systematic error of the centroid extraction, which fortunately can be corrected after the system calibration.

Let $\mathbf{P}_c = [x_c \ y_c \ z_c]^T$ denotes a reference point in the camera coordinate system. Then its actual projection on the camera image plane, denoted by \mathbf{P}_i^c , can be obtained by feeding \mathbf{P}_c into the camera model. And the centroid of the mark region has its projection $(\mathbf{P}_n^c)^*$ on the normalized image plane expressed by [7]

$$(\mathbf{P}_n^c)^* = \begin{bmatrix} (x_n^c)^* \\ (y_n^c)^* \end{bmatrix} = \begin{bmatrix} \frac{(x_c z_c + r^2 n_x n_z)}{z_c^2 + r^2(n_z^2 - 1)} \\ \frac{(y_c z_c + r^2 n_y n_z)}{z_c^2 + r^2(n_z^2 - 1)} \end{bmatrix}, \quad (12)$$

where r is the mark radius, $n_c = [n_x \ n_y \ n_z]^T$ is the normal of the reference point in the camera coordinate

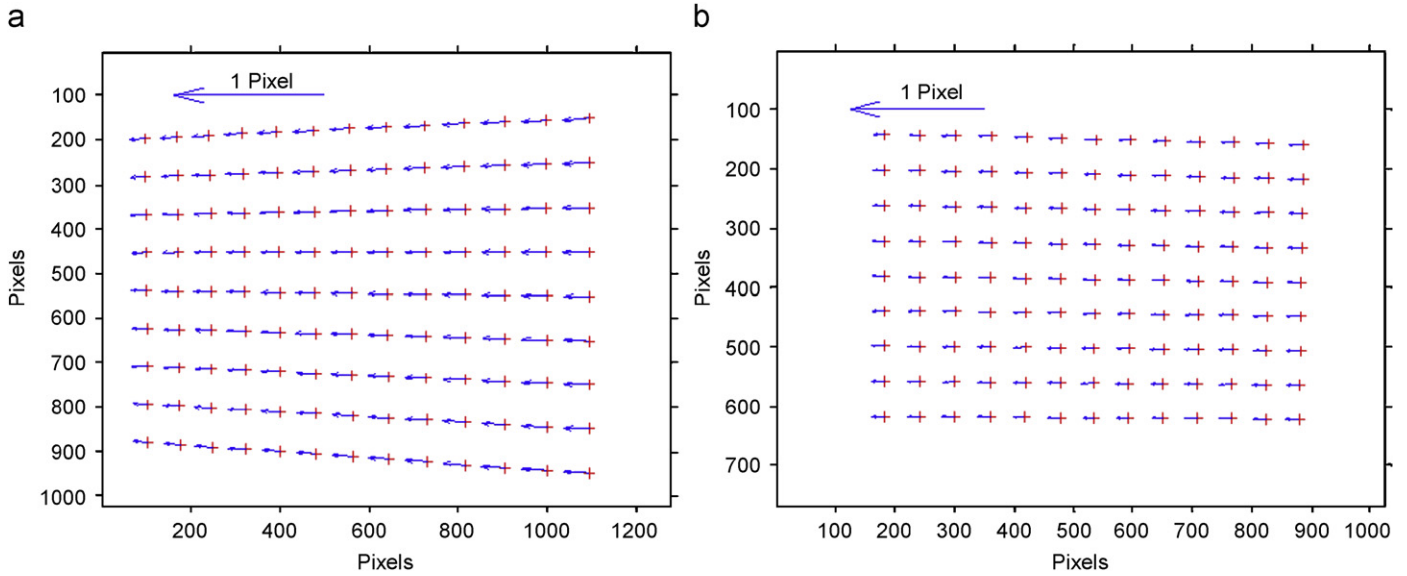


Fig. 8. Systematic error of centroid extraction for (a) camera and (b) projector.

system. Since n_c is along $-Z$ axis in WCS, we have

$$n_c = [n_x \ n_y \ n_z]^T = R_c \cdot [0 \ 0 \ -1]^T. \quad (13)$$

Substituting $(P_n^c)^*$ into Eqs. (3) and (4), the centroid of the mark region $(P_i^c)^*$ can be obtained. So the systematic error Δ is given by

$$\Delta = (P_i^c)^* - P_i^c. \quad (14)$$

This systematic error can be eliminated by subtracting Δ from the centroids previously extracted. And the projector correspondences are adjusted accordingly. Fig. 8 shows an example of the systematic error in our experiments. The normal of the error of the camera is 0.1375 ± 0.0276 pixels and that of the projector is 0.0956 ± 0.0049 pixels. After that, the system parameters can be refined by the system recalibration based on the corrected reference data.

4. Experiments and discussions

Our experiments utilize a 1280×1024 CCD camera, a 1024×768 LCD projector and the mechanism system of a Replica 3D Scanner. And the circular marks on the calibration board are equally distributed with the distance of 30 mm. When the mechanism translates the board along Z axis with each step of 30 mm, a $13 \times 9 \times 9$ 3D lattice of reference points covering a calibration volume of $360 \times 240 \times 240$ mm can be accomplished. Then the system calibration can be carried out as described in Section 3. In order to evaluate the performance improvement, we also calibrated the system with the conventional method [14,23–25] by simply projecting an extra calibration pattern with known circular marks onto the board for each step. Then the 3D positions of the projected circular mark centers on the board $P_w(k')$, where k' is the number of the points extracted, are determined by the camera parameters

which can be calibrated with the reference points $P_w(k)$ and their correspondences on the camera image plane $P_c(k)$. Thus, the projected circular mark centers $P_w(k')$, combined with the known circular mark centers on the extra calibration pattern, can be used to calibrate the projector.

Table 1 shows the calibrated system parameters by both our proposed method and the conventional method. As we can see, the projector parameters differ obviously for these two methods while the camera parameters are almost the same. It is because the reference data for the projector in the conventional method is not reliable for the reason of the influences from the camera calibration error. Fig. 9(a) and (b) shows the re-projection error of the reference points $P(k)$ onto the camera and projector image planes using the calibration results by our proposed method. The re-projection error of the projector is 0.1133 ± 0.0727 pixels, which is almost 2/3 smaller than that of the camera, 0.3274 ± 0.2134 pixels. This indicates that the device model can better describe the imaging process of the projector than that of the camera. Fig. 9(c) and (d) shows the re-projection error of the reference points $P(k)$ using the calibration results by the conventional method in compare. The camera re-projection error remains the same as that of our method. But the projector re-projection error is four times larger than that of our method and is more dispersed which also indicates the influences from the camera calibration error.

Distance measurement is carried out to evaluate the performance of our calibration method. The standard distances are obtained by simply pasting a circular mark on the moving mechanism of the Replica/Reversa 3D laser scanner and the mechanism translates the mark center at certain distance of 25 mm in space constructing a $9 \times 7 \times 5$ 3D lattice within the volume of $200 \times 150 \times 100$ mm. The 3D positions of the mark center, as the 3D lattice nodes, are reconstructed and the total number of 1152 distances

Table 1
Calibration results of the camera and projector

Method	Device	$f_u f_v$	$u_0 \ v_0$	$\mathbf{K} = \begin{bmatrix} k_1 & k_3 \\ k_2 & k_4 \end{bmatrix}$	\mathbf{R}_{pc}	\mathbf{T}_{pc}			
Proposed method	Camera	3070.42029	526.64139	−0.01599	−0.09081	0.8414	−0.0019	0.5404	−490.45371
		3037.22681	422.75774	−0.00728	−0.02535	−0.0108	0.9997	0.0203	180.97388
	Projector	1762.03883	503.85993	−0.01350	0.13538	−0.5403	−0.0230	0.8412	232.44547
		1755.04405	695.74382	0.00293	0.00244				
Conventional method	Camera	3070.42067	526.63960	−0.01599	−0.09080	0.8562	0.0066	0.516	−489.19600
		3037.22692	422.75851	−0.00728	−0.02535	−0.0124	0.9999	0.0079	180.37942
	Projector	1758.92551	455.55027	0.01724	0.01634	−0.5165	−0.0132	0.85662	232.96557
		1749.96386	672.37723	−0.00097	−0.00978				

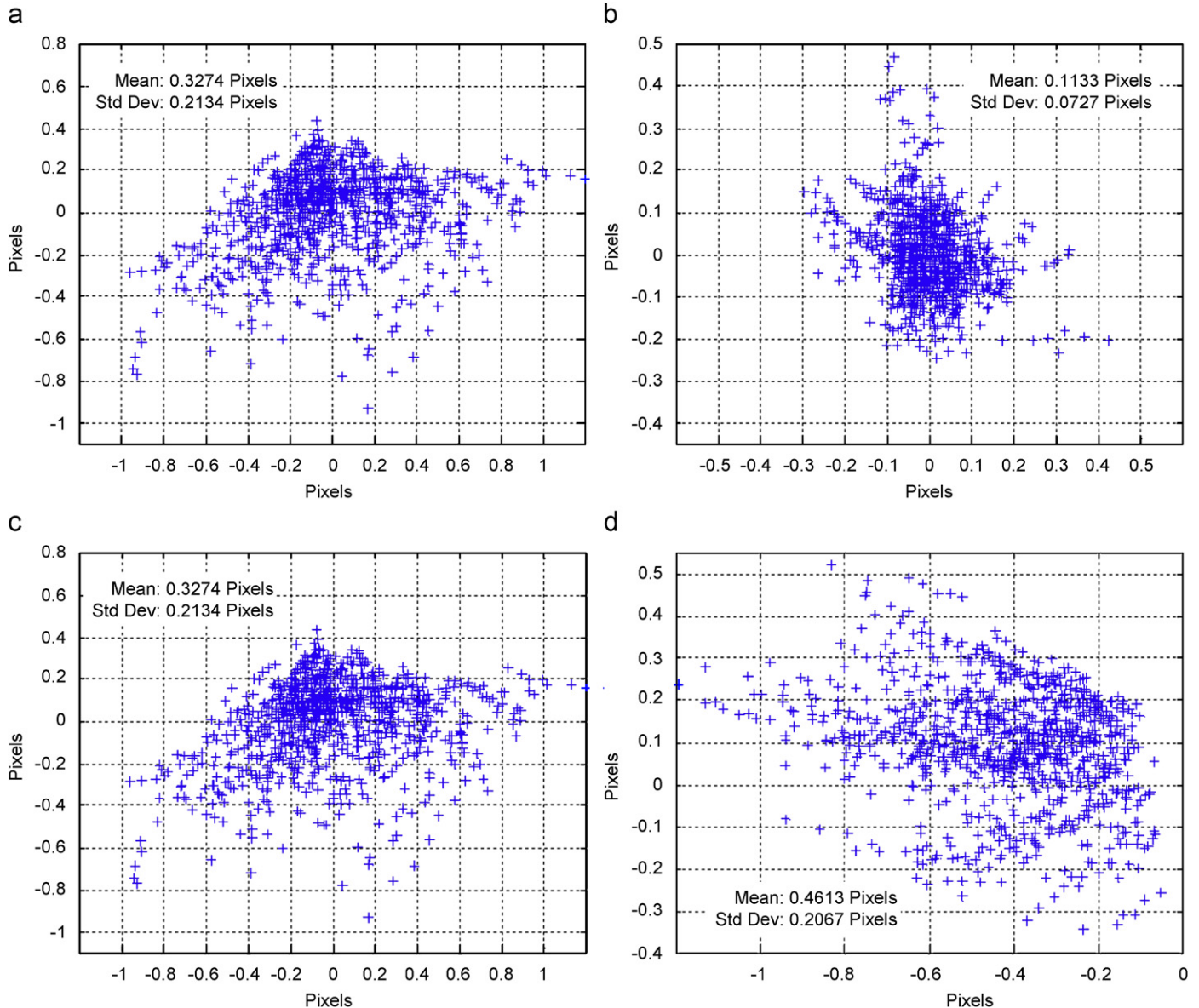


Fig. 9. Re-projection error of the reference points on (a) camera (b) projector image planes by our method, (c) camera and (d) projector image planes by the conventional method.

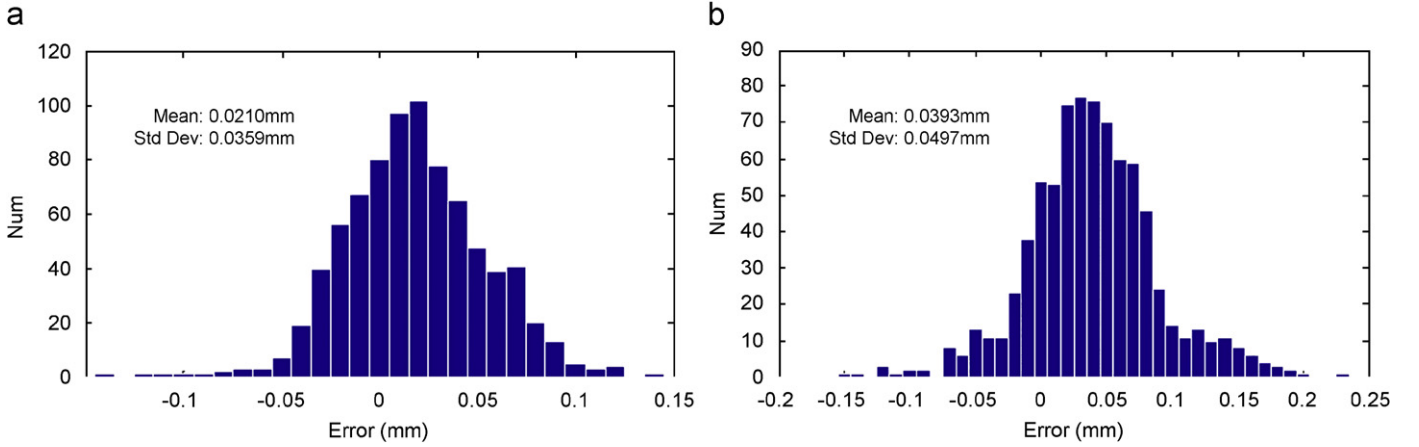


Fig. 10. Histogram of the measurement error of the 25 mm distances by: (a) our method and (b) conventional method.

between any two adjacent nodes can be calculated. Fig. 10 shows the histogram of the distribution of the distance measurement error. It is 0.0210 ± 0.0359 mm for our calibration method and is 0.0393 ± 0.0497 mm for the conventional method. We obtain 47% improvement for the measurement accuracy and 28% improvement for the uncertainty.

5. Conclusions

This paper proposes an accurate and systematic calibration method to improve the measurement accuracy of a camera–projector measurement system based on structured light projection. Our efforts improve three key factors in the system calibration: calibration model, calibration artifact and calibration procedures. And this calibration method enables the camera and projector calibration accomplished simultaneously using the same uniformly distributed 3D reference points based on the calibration model considering high to fourth order radial and tangential lens distortion. With our calibration method, the system measurement accuracy is improved by 47%, as demonstrated in the distance measurement experiment.

Acknowledgments

This work was supported by National Natural Science Foundation of China (Project no. 50575139), Shanghai Special Fund of Informatization (Project no. 088) and Programme of Introducing Talents of Discipline to Universities (Project no. B06012).

Appendix

A.1 Inverse camera model

The main point of the inverse camera model proposed in Refs. [16,26] is to iteratively approximate the projection of \mathbf{P}_i^c on the camera normalized image plane, denoted by \mathbf{P}_n^c , from the projection of \mathbf{P}_i^c on the camera norma-

lized image plane, denoted by \mathbf{P}_d^c . This process can be expressed by

$$\mathbf{P}_n^c \approx \mathbf{P}_d^c - f_d(\mathbf{P}_d^c, \mathbf{K}_c) \approx \mathbf{P}_d^c - f_d(\mathbf{P}_d^c - f_d(\mathbf{P}_d^c, \mathbf{K}_c), \mathbf{K}_c) \approx \dots, \quad (15)$$

where \mathbf{K}_c is the camera lens distortion, $f_d(\cdot)$ is the distortion function given in Eq. (3). The residual error can be within $1e-4$ pixels after 2–3 iterations, which is sufficient for the accurate 3D reconstruction.

A.2 3D reconstruction

After \mathbf{P}_n^c is obtained by the inverse camera model, the line vector $\mathbf{P}_l = [x_P \ y_P \ z_P]^T$ along the line $\mathbf{O}_c \mathbf{P}_i^c$ in the projector coordinate system can be expressed by

$$\mathbf{P}_l : \mathbf{R}_{pc} \begin{bmatrix} \mathbf{P}_n^c \\ 1 \end{bmatrix} \lambda + \mathbf{T}_{pc}, \quad (16)$$

where $\lambda \in \mathbb{R}$, \mathbf{R}_{pc} and \mathbf{T}_{pc} are given in Eqs. (10) and (11).

The projection of \mathbf{P}_l onto the projector image plane needs to satisfy the following equation:

$$g_u(P_l, \Theta'_p) - u_p^* = 0, \quad (17)$$

where $g_u(\cdot)$ calculates the first element of the device imaging process $g(\cdot)$ described in Eq. (5), $\Theta'_p = [\mathbf{I}(3) \ [0 \ 0 \ 0]^T \ f_u^p \ f_v^p \ u_0^p \ v_0^p \ \mathbf{K}_p]$ are part of the projector parameters and $\mathbf{I}(3)$ is the identity matrix of the size three.

Eq. (17) is a nonlinear equation and can be solved numerically by Newton–Raphson method [27]. The initial line vector \mathbf{P}_l^* is obtained by simply calculating the intersection point of \mathbf{P}_l and the plane defined by u_p^* discarding the projector lens distortion. The plane in the projector coordinate system is given by

$$\frac{u_p^* - u_0^p}{f_u^p} = \frac{x_P}{z_P}. \quad (18)$$

Solving Eqs. (16) and (18), \mathbf{P}_l^* can be obtained, thus the 3D position of \mathbf{P}_w can be reconstructed by solving Eq. (17).

The convergent speed is very fast and normally 4–6 iterations are enough to reach a residue of $1e-4$ pixels.

References

- [1] Chen F, Brown GM, Song M. Overview of three-dimensional shape measurement using optical methods. *Opt Eng* 2000;39(1):10–22.
- [2] Blais F. Review of 20 years of range sensor development. *J Electron Imaging* 2004;13(1):231–43.
- [3] Dhond UR, Aggarwal JK. Structure from stereo—a review. *IEEE Trans Syst, Man Cybernet* 1989;19(6):1489–510.
- [4] Aguilar JJ, Torres F, Lope MA. Stereo vision for 3D measurement: accuracy analysis, calibration and industrial applications. *Measurement* 1996;18(4):193–200.
- [5] Idesawa M. High-precision image position sensing methods suitable for 3-D measurement. *Opt Lasers Eng* 1989;10(3–4):191–204.
- [6] Keferstein CP, Marxer M. Testing bench for laser triangulation sensors. *Sens Rev* 1998;18(3):183–7.
- [7] Valkenburg RJ, McIvor AM. Accurate 3D measurement using a structured light system. *Image Vision Comput* 1998;16(2):99–110.
- [8] Pages J, Salvi J, Garcia R, Matabosch C. Overview of coded light projection techniques for automatic 3D profiling. In: *Proceedings of IEEE international conference on robotics and automation*, 2003. Taipei, Taiwan: Institute of Electrical and Electronics Engineers Inc.; 2003. p. 133–38.
- [9] Huang PS, Zhang S. Fast three-step phase-shifting algorithm. *Appl Opt* 2006;45(21):5086–91.
- [10] Greivenkamp JE, Bruning JH. Phase shifting interferometers. In: Malacara D, editor. *Optical shop testing*. New York: Wiley Express; 1992. p. 501–98.
- [11] Takasaki H. Moire topography. *Appl Opt* 1970;9(6):1467–72.
- [12] Sansoni G, Carocci M, Rodella R. Three-dimensional vision based on a combination of gray-code and phase-shift light projection: analysis and compensation of the systematic errors. *Appl Opt* 1999;38(31):6565–73.
- [13] Wiora G. High resolution measurement of phase-shift amplitude and numeric object phase calculation. In: *Proceedings of SPIE: vision geometry IX*, 2000. San Diego, CA, USA: Society of Photo-Optical Instrumentation Engineers, Bellingham, WA, USA; 2000. p. 289–99.
- [14] Sadlo F, Weyrich T, Peikert R, Gross M. A practical structured light acquisition system for point-based geometry and texture. In: *Symposium on point-based graphics*, 2005. Stony Brook, NY: Institute of Electrical and Electronics Engineers Inc., Piscataway, NJ 08855-1331; 2005. p. 89–98.
- [15] Tsai RY. A versatile camera calibration technique for high accuracy 3D machine vision metrology using off-the-shelf TV cameras and lenses. *J Rob Autom* 1987;RA-3(4):323–44.
- [16] Heikkila J, Silven O. Four-step camera calibration procedure with implicit image correction. In: *Proceedings of the conference on computer vision and pattern recognition*, 1997. San Juan, PR, USA: IEEE, Los Alamitos, CA, USA; 1997. p. 1106–12.
- [17] Zhang ZY. Flexible camera calibration by viewing a plane from unknown orientations. In: *Proceedings of the IEEE international conference on computer vision*, 1999. Kerkira, Greece: Institute of Electrical and Electronics Engineers Inc., Piscataway, NJ, USA; 1999. p. 666–73.
- [18] Bouguet JY. Camera calibration toolbox for Matlab, <www.vision.caltech.edu/bouguetj/calib_doc>.
- [19] Chen XB, Xi JT, Jin Y, Xu B. Accuracy improvement for 3D shape measurement system based on gray-code and phase-shift structured light projection. In: *Proceedings of SPIE: the fifth international symposium on multispectral image processing and pattern recognition*, 2007.
- [20] Zhang ZY. Camera calibration with one-dimensional objects. *IEEE Trans Pattern Anal Machine Intell* 2004;26(7):892–9.
- [21] Sturm PF, Maybank SJ. On plane-based camera calibration: a general algorithm, singularities, applications. *Proc IEEE Comput Soc Conf Comput Vision Pattern Recognit* 1999;1:432–7.
- [22] Heikkila J. Geometric camera calibration using circular control points. *IEEE Trans Pattern Anal Machine Intell* 2000;22(10):1066–77.
- [23] Ito M, Ishii A. Three-level checkerboard pattern (TCP) projection method for curved surface measurement. *Pattern Recognit* 1995;28(1):27–40.
- [24] Gockel T, Azad P, Dillmann R. Calibration issues for projector-based 3D-scanning. In: *Proceedings of IEEE: shape modeling international SMI 2004*, 2004. Geneva, Italy: IEEE Computer Society, Los Alamitos, CA 90720-1314, United States; 2004. p. 367–70.
- [25] Tsai MJ, Hung CC. Development of a high-precision surface metrology system using structured light projection. *Measurement* 2005;38(3):236–47.
- [26] Legarda-Saenz R, Bothe T, Juptner WP. Accurate procedure for the calibration of a structured light system. *Opt Eng* 2004;43(2):464–71.
- [27] Press WH, Teukolsky SA, Vetterling WT, Flannery BP. *Numerical recipes in C*. 2nd ed. Cambridge: Cambridge University Press; 1992.
- [28] Gonzalez RC, Woods RE. *Morphological image processing*. In: *Digital image processing*. 2nd ed. New York: Prentice-Hall; 2002. p. 519–66.